

# Crystallographic, Quantum Chemical and Molecular Docking Analysis of a Benzoic Acid Derivative

D Singh<sup>a</sup>, R Sharma<sup>a</sup>, S M Deshmukh<sup>b</sup>, S Murugavel<sup>c</sup>, D Lakshmanan<sup>d</sup> & R Kant<sup>a\*</sup>

<sup>a</sup>Chemical Crystallography Laboratory, Department of Physics, University of Jammu, Jammu Tawi 180 006, India

<sup>b</sup>Department of Chemistry, Dr. B. R. Ambedkar National Institute of Technology, Jalandhar, Punjab 144 011, India

<sup>c</sup>Department of Physics, Thanthai Periyar Government Institute of Technology, Vellore, Tamil Nadu 632 002, India

<sup>d</sup>Department of Physics, C. Abdul Hakeem College of Engineering and Technology, Melvisharam, Vellore, Tamil Nadu 632 509, India

Received 6 July 2023; accepted 10 August 2023

The compound 2-(3-phenyl)-5-((m-toluloxo) methyl)-4H-1,2,4-triazole-4-yl) benzoic acid (PTMTBA) has been characterized using various analytical techniques such as NMR, FT-IR, and single crystal X-ray diffraction. The molecular structure reveals some fascinating features. The O1—H1...N4 and C—H... $\pi$  intermolecular hydrogen bonding between molecules constitute a three-dimensional molecular network. The crystal structure has been optimized using both Hartree-Fock (HF) and Density functional theory (DFT) calculations. The molecular electrostatic potential (MEP) and frontier molecular orbitals (FMOs) of the molecule have been analyzed to gain insight into its physical and chemical properties. 3D Hirshfeld surfaces and allied 2D fingerprint plots have been analyzed for molecular interactions. The molecule docks very well with the target protein (PDB code: 3FFP), indicating it to be an effective inhibitor of carbonic anhydrase.

**Keywords:** X-ray diffraction; Hydrogen bonds; DFT; Hirshfeld surface; Interaction energy; Molecular docking

## 1 Introduction

Triazole and its derivatives have attracted considerable attention for the past few decades due to their chemotherapeutic value<sup>1,2</sup>. The compounds with a triazole nucleus exhibit a variety of biological activities<sup>3-7</sup> and properties that aid the production of insulin, treat acute neurological disorders, regulate nucleoside metabolism, and alleviate asthma attacks<sup>8</sup>.

The structural characterization of 2-(3-phenyl)-5-((m-toluloxo) methyl)-4H-1,2,4-triazole-4-yl) benzoic acid (PTMTBA) is being reported using IR, <sup>1</sup>H NMR, SCXRD, and DFT/HF techniques. The DFT method has been employed to determine the chemical reactivity, structural characteristics, and Hirshfeld surfaces. The molecular electrostatic potential (MEP) and the frontier molecular orbitals (FMOs) analyses have been made. The intermolecular interactions existing in the crystal structure are characteristic of the Hirshfeld surface analysis. The molecular docking analysis has also been performed to assess its application potential.

## 2 Materials and Methods

### 2.1 Synthesis

It involves the reaction of anthracitic acid (0.07mol) with benzoyl chloride (0.15mol) in pyridine. The reaction mixture is stirred well, followed by the neutralization with 5% aqueous sodium bicarbonate to get solid 2-phenyl 1,3-oxazine (m.p.120 °C), which, on further reaction with m-methyl phenoxyacetic acid hydrazide in refluxing methanol on an oil bath for 3 hours, gave the desired crystalline solid. Yield 60%, m.p. 220 °C. IR (KBr):  $\nu_{\max}$ , 3520-3300 broad (-OH), 1705-1680(C=O), 1620(C=N), 1600(C=C) cm<sup>-1</sup>. PMR (DMSO-d<sub>6</sub>):  $\delta$ , 12.5 (1H, singlet br, OH), 6.8-7.6 (13H, m, aromatic protons), 4.65 (2H, s, OCH<sub>2</sub>), 2.3 (3H, s, aromatic CH<sub>3</sub>) ppm.

### 2.2 Structure determination

The SuperNova single crystal X-ray diffractometer has been used for the intensity data collection at 293(2) K using MoK $\alpha$ -radiation ( $\lambda=0.71073\text{\AA}$ ). Using Olex2<sup>9</sup>, the structure has been solved with ShelXT<sup>10</sup> (using Intrinsic Phasing) and refined with ShelXL<sup>11</sup> (using Least-Squares minimization). All the H-atoms were placed at the chemically acceptable positions.

\*Corresponding author: (E-mail: rkant.ju@gmail.com)

264 parameters, refined with 4369 distinct reflections, converged the  $R=0.0503$  ( $wR^2=0.124$ ). The crystal data are summarized in Table 1. An ORTEP view of the molecule is shown in Fig. 1<sup>12</sup>.

### 2.3 Theoretical studies

The quantum chemical calculations were performed using HF and DFT/B3LYP method with the basis set 6-311++ G (d, p) (Gaussian 09 program)<sup>13</sup>. Using the optimized structure, the geometrical parameters, HOMO-LUMO, and MEP were investigated. The Hirshfeld surfaces (HSs), 2D fingerprint plots (FPs), and intermolecular interaction energies were calculated using the Crystal Explorer 21.5<sup>14</sup>. The molecular docking has been performed using the AutoDock Vina software<sup>15</sup>. The target protein carbonic anhydrase II (PDB ID: 3FFP) file was downloaded from the RCSB protein data bank<sup>16</sup>. The coordinates of the active site of the protein were  $X = -6.98$ ,  $Y = 1.25$ , and  $Z = 16.27$ . The complete ligand-protein interactions were visualized using Discovery Studio 4.1 Visualizer software<sup>17</sup>.

Table 1 — Crystal and structure-refinement data for PTMTBA

CCDC number	2240419
Empirical formula	$C_{23}H_{19}N_3O_3$
Formula weight	385.41
Crystal system, space group	Orthorhombic, Pbc <sub>a</sub>
Lattice parameters a, b, c, $\beta$	$a = 16.076(6)\text{\AA}$ , $13.554(5)\text{\AA}$ , $18.526(8)\text{\AA}$ , $90^\circ$
Volume, Z	$4036.8(3)\text{\AA}^3$ , 8
Calculated density	$1.268\text{ Mg/m}^3$
Absorption coefficient	$0.086\text{ mm}^{-1}$
F(000)	1616
Theta range for data collection	$3.20$ to $27.41^\circ$
Limiting indices h, k, l	$-20 \rightarrow 20$ , $-13 \rightarrow 17$ , $-23 \rightarrow 23$
Reflections collected / unique	4369 / 2900
Data / restraints / parameters	2900 / 0 / 264
Final R indices [ $I > 2\sigma(I)$ ]	$R1 = 0.0503$ , $wR^2 = 0.1240$
R indices (all data)	$R1 = 0.0819$ , $wR^2 = 0.1407$
Largest diff. peak and hole	$0.249$ and $-0.257\text{ e}\text{\AA}^{-3}$
Goodness-of-fit on $F^2$	1.045

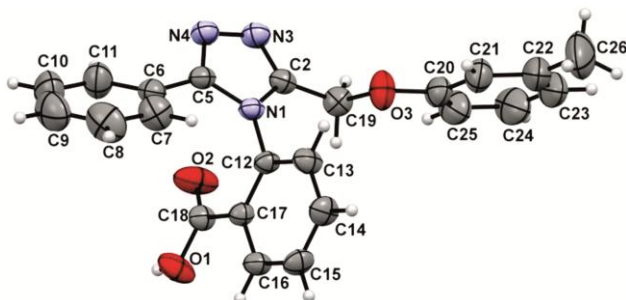


Fig. 1 — An ORTEP view of the molecule with atomic numbering scheme.

## 3 Results and Discussion

### 3.1 Molecular structure analysis

The N—N and C—N bond distances in the triazole ring are comparable with some analogous structures<sup>18-21</sup>. The dihedral angle between the triazole ring and phenyl acetic acid is  $76.11^\circ$ , while it is  $74.71^\circ$  between the triazole and the methoxy phenyl ring. Both these dihedral angles are axially oriented. The crystal packing is stabilized by O1—H1...N4 and C—H... $\pi$  intermolecular hydrogen bonds and C16—H16...O1 intramolecular bonds (Fig. 2) (Table 2). The optimized geometrical parameters as obtained using the HF/DFT method are close to the XRD measurement.

### 3.2 MEP and HOMO-LUMO energy gap

The negative region in MEP (Fig. 3(a)) is mainly focused on the atoms N3 and N4, with the highest red colour intensity caused by the contribution of lone-pair electrons, inferring that these are suitable sites for electrophilic attack. The areas of the structure that are pale red or yellow are the sites representing weak

Table 2 — Hydrogen bond geometry of PTMTBA

D—H...A	D—H	H...A	D...A	D—H...A
C16—H16...O1	0.93	2.39	2.712(2)	165
O1—H1...N4 <sup>i</sup>	0.82	1.84	2.638(2)	100
C7—H7...Cg4 <sup>ii</sup>	0.82	3.22	3.561(2)	104
C10—H10...Cg4 <sup>iii</sup>	0.93	3.21	3.964(2)	140
C14—H14...Cg1 <sup>iv</sup>	0.93	3.13	4.055(2)	174
C24—H24...Cg3 <sup>v</sup>	0.93	2.90	3.759(2)	153

Symmetry codes: i)  $1/2-x, -1/2+y, z$  ii)  $x, 1/2-y, 1/2+z$  iii)  $-1/2+x, y, 1/2-z$  iv)  $1/2+x, y, 1/2-z$  v)  $1-x, -y, -z$ . Cg1, Cg3 and Cg4 represent the centroid of (N1—C5), (C12—C17) and (C20—C25) rings, respectively.

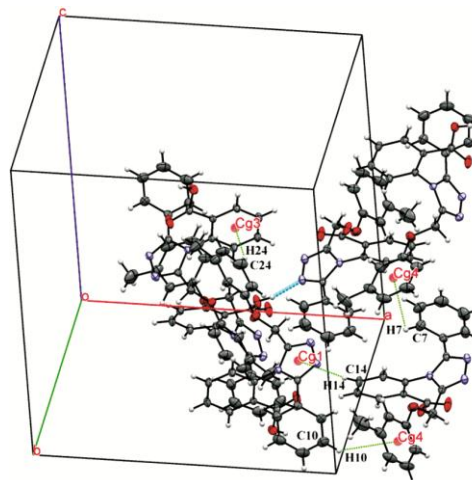


Fig. 2 — Unit cell packing showing various intermolecular interactions.

interactions. The positive potential sites (blue colour) are around the hydrogen atoms of the OH group, suggesting their nucleophilic nature.

The HOMO and LUMO energy values are -6.303 eV and -2.243 eV, respectively, while the energy gap is 4.06 eV. The important global reactivity parameters and their corresponding values are presented in Table 3. A molecule with a large energy gap is less reactive and has high kinetic stability, which is known as a hard molecule. The atomic orbital mechanism for the frontier molecular orbitals is shown in Fig. 3(b).

### 3.3 Hirshfeld surfaces, 2D fingerprint plots and energy framework analysis

The Hirshfeld surface mapping of the  $d_{\text{norm}}$  and shape index reveals information about additional weak interactions that are present in the molecule. In Fig. 4(a), the red area represents O—H...N

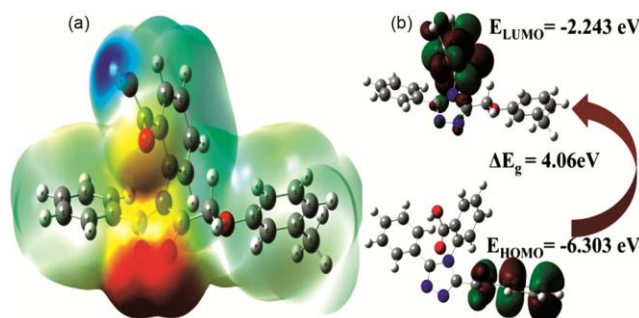


Fig. 3 — (a) Molecular electrostatic potential (MEP) map and (b) HOMO-LUMO energy gap.

Table 3 — The calculated parameters (eV) of the PTMTBA using DFT approach.

Property	Symbol and formula	Value (eV)
E(HOMO)	$E_H$	-6.30
E(LUMO)	$E_L$	-2.24
Orbital energy gap	$\Delta E = (E_L - E_H)$	4.06
Ionization potential	$-E_H$	6.30
Electron affinity	$-E_L$	2.24
Electronegativity	$\chi = -\mu$	4.27
Hardness	$\eta = (E_L - E_H)/2$	2.03
Softness	$S = 1/2\eta$	0.25 (eV <sup>-1</sup> )

connections, whereas the blue area represents weak interactions. On the shape index surface [Fig. 4(b)], the C—H... $\pi$  interactions indicate red patches that surround the atoms actively participating in the interaction.

Two-dimensional fingerprint plots and their subdivision into H...H, H...C/C...H, H...O/O...H, H...N/N...H, and C...C contacts are shown (Fig. 5), together with their respective contributions to the Hirshfeld surface.

The total interaction energy (-239.3 kJ/mol) is comprised of four components: electrostatic (-139.6 kJ/mol), polarisation (-39.5 kJ/mol), dispersion (-221.6 kJ/mol) and repulsion energy (211 kJ/mol) (Table 4).

### 3.4 Molecular docking analysis

The binding pose of the PTMTBA at the binding site of the 3FFP enzyme is shown in Fig. 6(a). The two-dimensional binding interaction of the compound with carbonic anhydrase II binding sites is shown in Fig. 6(b). The binding energy, distance, and bonding types are listed in Table 5.

The PTMTBA-3FFP complex is stabilized by three conventional hydrogen bonds, one electrostatic bond, and six hydrophobic bond interactions. The two hydrophobic interactions (Pi-Sigma) between ILE91

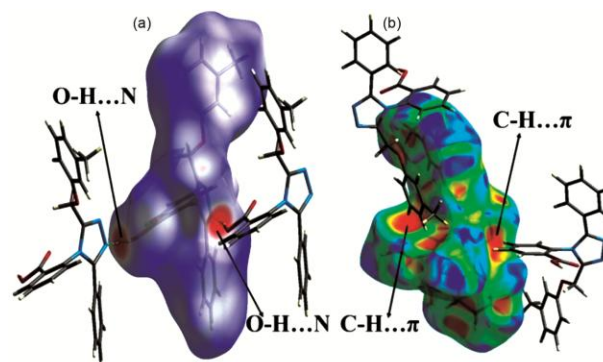


Fig. 4 — (a) Hirshfeld surface mapped over  $d_{\text{norm}}$  and (b) Shape index plot.

Table 4 — Different interaction energies of the molecules pairs in kJ/mol calculated at B3LYP/6-31G (d, p) basis set.

N	Symp	R	E_ele	E_pol	E_dis	E_rep	E_tot
2	x, -y+1/2, z+1/2	10.34	-2.4	-2.0	-29.2	12.1	-21.9
2	-x+1/2, -y, z+1/2	11.09	-4.0	-0.8	-11.0	2.9	-12.5
1	-x, -y, -z	10.79	-3.9	-0.6	-24.6	14.6	-16.9
2	x+1/2, y, -z+1/2	8.10	-15.4	-5.1	-34.3	20.7	-37.2
2	-x, y+1/2, -z+1/2	7.25	-15.1	-3.9	-40.1	29.5	-35.5
1	-x, -y, -z	8.83	-9.9	-1.5	-57.4	33.6	-40.8
2	-x+1/2, y+1/2, z	8.85	-80.3	-21.9	-14.2	97.6	-53.2
2	x+1/2, -y+1/2, -z	12.39	-8.6	-3.7	-10.8	0.0	-21.3

Table 5 — Binding energy, Hydrogen bond, Electrostatic and Hydrophobic contacts of PTMTBA to 3FFP.

Inhibitor	Binding Energy (Kcal mol <sup>-1</sup> )	Interactions	Distance (Å)	Bonding	Bonding Types
(a*)	-9.4	ASN62[H...O]	2.294	HB	Conventional
		ASN62[H...O]	2.939	HB	Conventional
		ASN67[H...O]	2.854	HB	Conventional
		HIS94[N...π]	4.443	Electrostatic	Pi-Cation
		ILE91 [CH...π]	3.767	Hydrophobic	Pi-Sigma
		LEU198[CH...π]	3.549	Hydrophobic	Pi-Sigma
		PHE131[π...π]	4.879	Hydrophobic	Pi-Pi Stacked
		HIS94[π...π]	4.990	Hydrophobic	Pi-Pi T-shaped
		VAL121[C...π]	4.447	Hydrophobic	Pi-Alkyl
		VAL121[C...π]	5.121	Hydrophobic	Pi-Alkyl

(a\*) = 2-(3-phenyl)-5-((m-toluxoy) methyl)-4H-1,2,4-triazole-4-yl) benzoic acid

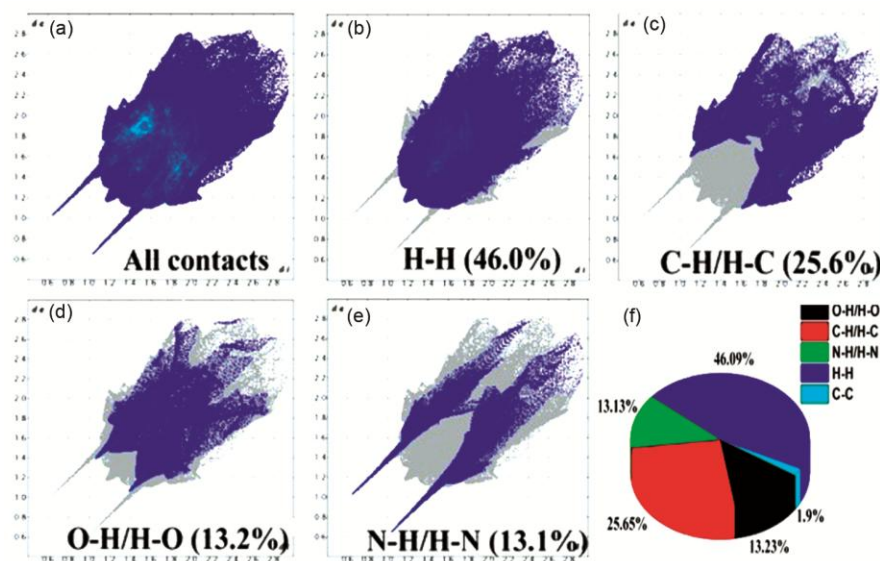


Fig. 5 — Fingerprint plots for PTMTBA illustrating the contributions to the total HS of the various contacts.

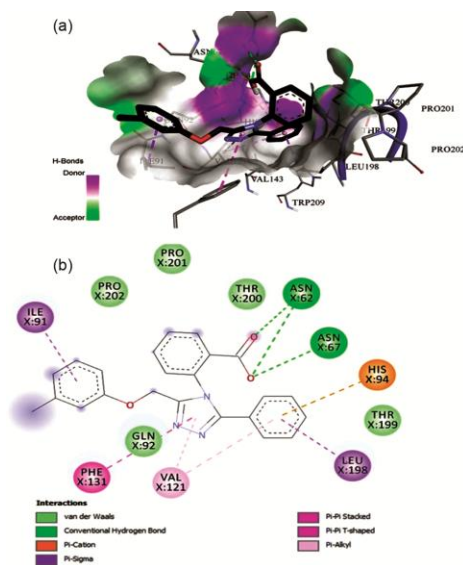


Fig. 6 — (a) Molecular binding interaction of PTMTBA to 3FFP binding site and (b) The 2D binding interaction of PTMTBA to 3FFP binding site.

and LEU198 are bonded with two benzene rings of the ligand at a distance of 3.767 Å and 3.549 Å, respectively. The hydrophobic interaction (Pi-Pi stacked) occurs between the triazole ring and the six membered ring of residue PHE131 at a distance of 4.879 Å. The (Pi-Pi T-shaped) hydrophobic interaction occurs between the six-membered rings of the ligand and the five-membered ring of residue HIS94 at a distance of 4.99 Å. The high binding energy score and a greater number of interactions confirm that the molecule has the potential to act as a potent inhibitor for carbonic anhydrase II.

#### 4 Conclusion

The synthesis and structural characterization of 2-(3-phenyl)-5-((m-toluxoy) methyl)-4H-1,2,4-triazole-4-yl) benzoic acid, have been carried out using experimental and theoretical techniques. The O—H...N and C—H...π intermolecular interactions lend

stability to the molecules in the unit cell. The measured bond lengths and bond angles are in agreement with the corresponding theoretical values. The MEP surface reveals that the electron rich domains are predominantly clustered around the nitrogen atoms. The analysis of the Hirshfeld surface and 2D fingerprint plots reveals the nature of the interactions present in the molecule. The molecular docking analysis of the complex PTMTBA-3FFP indicates a highly favourable binding energy of -9.4 kcal/mol, suggesting that the molecule may potentially serve as a potent inhibitor for carbonic anhydrase II.

### Acknowledgement

DS is thankful to University of Jammu for extending the research facilities.

### References

- Holla B S, Manjathuru M, Mari S K, Boja P, Padiyath M A & Nalilu S K, *Eur J Med Chem*, 40 (2005) 1173.
- Sanghvi Y S, Bhattacharya B K, Kini G D, Matsumoto S S, Larson S B, Jolley W B, Robins R K & Revankar G R, *J Med Chem*, 33 (1990) 336.
- Guan L P, Jin Q H, Tian G R, Chai K Y & Quan Z S, *J Pharm Sci*, 10 (2007): 254.
- Padmavathi V, Reddy G S, Padmaja A & Kondaiah P, *Eur J Med Chem*, 44 (2009)2106.
- Zoumpoulakis P, Camoutsis C, Pairas G, Soković M, Glamočlija J, Potamitis C & Pitsas A, *Bioorg & Med Chem*, 20 (2012)1569.
- Dong W L, Liu Z X, Liu X H, Li Z M & Zhao W G, *Eur J Med Chem*, 45 (2010) 1919.
- Yang L, Wu Y, Yang Y, Wen C & Wan J P, *Beil J Org Chem*, 14 (2018) 2348.
- Deshmukh M B, Suryawanshi A W, Mali A R & Dhongade Desai S R, *Synt Comm*, 34 (2004) 2655.
- Dolomanov O V, Bourhis L J, Gildea R J, Howard J A & Puschmann H, *J Appl Crystallogr*, 42 (2009)339.
- Sheldrick G M, *Acta Crystallogr*, A71 (2015) 3.
- Sheldrick G M, *Acta Crystallogr*, C71 (2015) 3.
- Macrae C F, Bruno I J, Chisholm J A, Edgington P R, McCabe P, Pidcock E, Rodriguez-Monge L, Taylor R, Streek J V & Wood P A, *J Appl Crystallogr*, 41 (2008) 466.
- Frisch A, Gaussian 09W Reference, (Wallingford USA), (2009) 25.
- Spackman P R, Turner M J, McKinnon J J, Wolff S K, Grimwood D J, Jayatilaka D & Spackman M A, *J Appl Crystallogr*, 54 (2021) 1006.
- Morris G M, Huey R, Lindstrom W, Sanner M F & Belew R K, *J Comput Chem*, 30 (2009) 2785.
- <https://www.rcsb.org/>
- Biovia D S, Discovery studio visualizer, San Diego, C A, USA, (2017) 936.
- Palmer M H & Parsons S I, *Acta Crystallogr*, C52 (1996) 2818.
- Perman C A & Gleason W B, *Acta Crystallogr*, C47 (1991) 1018.
- Puviarasan K, Govindasamy L, Shanmuga Sundara Raj S, Velmurugan D, Jayanthi G & Fun H K, *Acta Crystallogr*, C55 (1999) 951.
- Rajakannan V, Govindasamy L, Velmurugan D, Sekar K, Senthilvelan A, Shanmuga Sundara Raj S & Fun H K, *Crys Res Tech: J Exp Indus Crystallogr*, 37 (2002) 301.